

A Recipe for Soft Fluidic Elastomer Robots

Andrew D. Marchese, Robert K. Katzschmann, and Daniela Rus*

December 9, 2014

Abstract

This work provides approaches to designing and fabricating soft fluidic elastomer robots. That is, three viable actuator morphologies composed entirely from soft silicone rubber are explored, and these morphologies are differentiated by their internal channel structure, namely: ribbed, cylindrical, and pleated. Additionally, three distinct casting-based fabrication processes are explored: lamination-based casting, retractable-pin-based casting, and lost-wax-based casting. Furthermore, two ways of fabricating a multiple DOF robot are explored: casting the complete robot as a whole, and casting single DOF segments with subsequent concatenation. We experimentally validate each soft actuator morphology and fabrication process by creating multiple physical soft robot prototypes.

1 Introduction

The goal of this work is to describe several fabrication methods for soft robots. Each method produces a unit-module that can be actuated in the soft fluidic elastomer model. The unit-modules can be composed to create different soft robot morphologies. We experimentally validate these in the context of extremely soft and highly compliant locomotory robots and manipulators shown in Figure 1. Each fabrication process can be used to create unit-actuatable soft modules; these modules can be composed in series or in parallel to create a range of soft robot morphologies.

Soft robots exhibit continuum body motion, large scale deformation, and relatively high compliance compared to traditional rigid-bodied robots [Trivedi et al., 2008]. Such characteristics give this class of robots advantages like the ability to mitigate uncertainty with passive compliance [McMahan et al., 2006], perform highly dexterous tasks [Deimel and Brock, 2014], and exhibit resiliency [Tolley et al., 2014b]. This work provides a recipe for designing and fabricating soft fluidic elastomer actuators and robotic systems.

Recent reviews [Trivedi et al., 2008, Trimmer, 2014, Lipson, 2014, Majidi, 2014] articulate the challenges associated with creating robots from soft, nonlinear materials. Current engineering tools are well-suited for rigid-bodied robots and

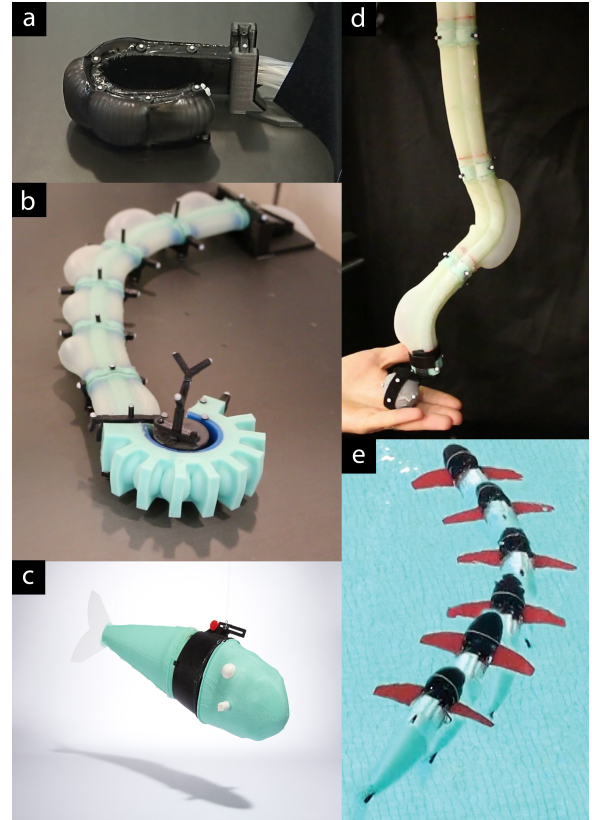


Figure 1: Extremely soft and highly compliant fluidic elastomer robots. (a) Ribbed planar manipulator [Marchese et al., 2014b], (b) Cylindrical manipulator with gripper [Katzschmann et al., 2015], (c) Self-contained pneumatic fish [Marchese et al., 2014c](photo courtesy of Devon Jarvis for popular mechanics), (d) Spatial cylindrical manipulator [Marchese and Rus, 2015], and (e) Self-contained hydraulic fish [Katzschmann et al., 2014].

when soft, nonlinear elastic materials are introduced, many of the underlying assumptions of these tools are broken. To create fluidic elastomer robots, we must overcome many technical challenges, many of which have to do with design and fabrication. More specifically, this work addresses the following challenges: (i) We need methods for composing soft-unit modules to create complex morphologies suitable for robot bodies capable of autonomous locomotion and manipulation. That is, we need to identify appropriate modules and ways of assembling these into multi-body robots. (ii) Consistently reproduc-

*Andrew D. Marchese, Robert K. Katzschmann, and Daniela Rus are with the Computer Science and Artificial Intelligence Laboratory, Massachusetts Institute of Technology, 32 Vassar St. Cambridge, MA 02139, USA, {andy, rkk, rus}@csail.mit.edu

ing certain properties of soft robots, for example their elasticity or internal channel geometry, is difficult using conventional fabrication techniques. Accordingly, we must develop fabrication techniques that balance the competing goals of scalability and repeatability with the need for complicated features and shape profiles.

This paper is organized as follows. First, we review relevant soft actuation technology, design tools, and fabrication processes in Section 2. Next, we present the design and characterization of three fluidic elastomer actuator morphologies in Section 3. These actuator morphologies are differentiated by their internal channel structure, namely: ribbed, cylindrical, and pleated. Next, we provide three alternative fabrication approaches for reliably fabricating soft actuators and multi-segment robots in Section 4. These processes are lamination-based embedded casting, retractable-pin-based casting, and lost-wax-based casting. Then, we briefly discuss alternative approaches to powering these robots in Section 5. And lastly, we demonstrate how the various actuator morphologies and fabrication processes have been used to realize a variety of soft autonomous systems: locomotory fish-like robots in Section 6 and robotic manipulation systems in Section 7.

Specifically, this work makes the following contributions:

1. Three fabrication processes for reliably manufacturing these FEAs. These are (i) a lamination-based casting process with heterogeneous embedded components, (ii) a retractable-pin-based casting process, (iii) a lost-wax-based casting process;
2. Three viable fluidic elastomer actuator (FEA) morphologies. That is, a FEA with a (i) ribbed channel structure and embedded transmission lines, (ii) cylindrical channel structure and hollow interior, (iii) seamless pleated channel structure;
3. A survey of recent robots built using these design and fabrication approaches (See Fig. 1).

This work significantly extends three previous conference publications: [Marchese et al., 2014b], [Marchese et al., 2014a], and [Katzschmann et al., 2015] (in revision).

2 Related Work

This paper builds on several recent results in the design and fabrication of soft robots; see [Lipson, 2013], [Rus and Tolley, 2014], [Marchese, 2014] for detailed reviews.

2.1 Actuation

There are various approaches to actuating the body of a soft robot. One distinguishing feature of many soft robots is that actuators and/or power transmission systems are integrated within and distributed throughout the body. In the following we review four common actuator types, and these are also depicted in Figure 2.

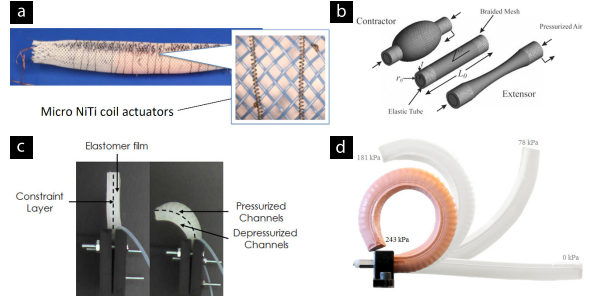


Figure 2: Common actuation approaches for soft robots. (a) Shape Memory Alloy (SMA) actuators [Seok et al., 2010], (b) Pneumatic Artificial Muscle (PAM) actuators [McMahan et al., 2006], (c) Fluidic Elastomer Actuators (FEAs) [Onal et al., 2011], and (d) Fiber reinforced FEAs [Galloway et al., 2013].

2.1.1 Tendons

Originally, many hard hyper redundant and hard continuum robots [Cieslak and Morecki, 1999, Buckingham, 2002, Gravagne and Walker, 2002, Hannan and Walker, 2003, McMahan et al., 2005, Camarillo et al., 2009] used an array of servomotors or linear actuators to pull cables that move rigid connecting plates located between body segments. Some softer robots have adopted a similar actuation scheme consisting of tendons pulling rigid fixtures embedded within an elastomer body. For example, the elastomer based bio-inspired octopus arm developed in Calisti et al. [2010], Laschi et al. [2012] and Calisti et al. [2011] uses Shape Memory Alloy (SMA) actuation. Further, Seok et al. [2010] use SMA actuators within a worm-like locomotory robot (see Fig. 2a). The basic operating principle behind SMA technology is that nickel titanium (NiTi) wire contracts under joule heating. This heating is typically produced by passing electrical current through the wire. The contracting wire can be used as an agonist actuator, similar to the way one's bicep pulls the forearm towards the body during a curl. There are also soft elastomer robots that use more traditional variable tension cables. For example, the soft-bodied fish developed by Valdivia y Alvarado and Youcef-Toumi [2006] as well as the soft arm developed by Wang et al. [2013] use this actuation approach, but these both consist of only one actuated segment.

2.1.2 Pneumatic Artificial Muscles

Another common actuation scheme for soft robots involves distributed Pneumatic Artificial Muscle (PAM) actuators (see Fig. 2b) also known as the McKibben actuator. A PAM is fundamentally composed of an inflatable elastic tube surrounded by a braided mesh. Depending on the weave pattern of the braided mesh the actuator can be designed to contract or extend under input pressure. Typically these actuators are operated with driving pressures between 50 and 100 psi. These actuators have been used and studied extensively in Chou and Hannaford [1996], Tondu and Lopez [2000] and Daerden and Lefever [2002]. Notable semi-soft robots using PAMs include

[McMahan et al., 2006, Pritts and Rahn, 2004] and Kang et al. [2013].

2.1.3 Fluidic Elastomer Actuators

A softer alternative is the Fluidic Elastomer Actuator (FEA), which is used predominantly throughout this paper (see Fig. 2c). The FEA is a bending actuator composed of low durometer rubber and driven by relatively low-pressure fluid, 3 to 8 psi. Its basic structure consists of two soft elastomer layers separated by a flexible but inextensible constraint. Each of these elastomer layers contains embedded fluidic channels. By pressurizing the fluid entrapped in these channels, stress is induced within the elastic material producing localized strain. This strain in combination with the relative inextensibility of the constraint produces body segment bending. FEAs can be powered pneumatically or hydraulically.

Perhaps the earliest application of pneumatically actuated elastomer bending segments to robotics was by Suzumori et al. [1992]. Here fiber-reinforced Flexible Microactuators (FMAs) were developed and shown viable in a manipulator and multi-fingered hand. Recently, these concepts have been extended and developed into the FEA and used to build a variety of soft mechanisms [Shepherd et al., 2011, Ilievski et al., 2011, Morin et al., 2012, Martinez et al., 2013, Marchese et al., 2014c,b,a, Katzschmann et al., 2014, Tolley et al., 2014a, Katzschmann et al., 2015, Marchese and Rus, 2015, Marchese et al., 2015a,b]. and soft robotic systems [Onal et al., 2011, Marchese et al., 2011, Onal and Rus, 2013, Marchese et al., 2014c,b,a, Katzschmann et al., 2014, Tolley et al., 2014a,b, Katzschmann et al., 2015, Marchese and Rus, 2015, Marchese et al., 2015a,b]. Actuators within these mechanisms and robots use elastomers of varying stiffness as well as cloth, paper, plastics, and even stiffer rubbers for their constraint layers. Furthermore, Polygerinos et al. [2013] and Mosadegh et al. [2014] have investigated more elaborate channel designs in order to reduce elastomer strain.

There are also less flexible, fiber-reinforced FEAs (see Fig. 2d) that occupy the soft actuator space between purely elastomer FEAs and PAMs. These actuators operate with driving pressures of between 25 and 35 psi and can accordingly apply higher forces which is an advantage for many applications. There are several notable examples of fiber-reinforced FEAs in the literature Suzumori et al. [1992, 2007], Bishop-Moser et al. [2012], Galloway et al. [2013], Deimel and Brock [2013, 2014] and Park et al. [2014].

2.2 Design Tools

Design tools for soft robots are limited with respect to the availability of design tools for more traditional rigid-body robots. Suzumori et al. [2007] use Finite Element Modeling (FEM) to analyze the bending of fiber reinforced pneumatic tube-like actuators. Specifically, hyperelastic material models are used to capture the nonlinear material properties of rubber, line elements are used to represent radial inextensibility constraints due to fiber reinforcement, and the simulation is per-

formed using the software MARC. Outside of this example, the community has generally found that iterative nonlinear finite element solvers are limited to small deformations and of limited use when modeling very soft nonlinear materials [Lipson, 2014]. VoxCAD and the Voxelyze physics engine, as used in Cheney et al. [2013] and Lehman and Stanley [2011] and reviewed by Lipson [2014], are simulation tools for very soft nonlinear materials. These tools use the concept of nonlinear relaxation to effectively perform physically correct particle-based material simulation. They have the advantage of allowing the user to individually set the local material properties of each particle. The disadvantage is that many physical parameters of active and passive material types must be experimentally derived.

2.3 Fabrication

Cho et al. [2009] review several manufacturing processes for soft biomimetic robots. The vast majority of soft elastomer robots rely on the processes of soft lithography [Xia and Whitesides, 1998] and/or shape deposition manufacturing [Cham et al., 2002]. Specifically, for soft fluidic elastomer robots this fabrication process generally consists of three steps as shown in Figure 3: (1) Two elastomer layers are molded through a casting process using pourable silicone rubber. The mold used for the outer layer contains a model of the desired channel structure. When cast, the outer layer contains a negative of this channel structure. The mold used for the constraint layer may contain fiber, paper, or a plastic film to produce the the inextensibility property required for actuation. When the elastomer is poured, this material is effectively embedded within the constraint layer. (2) The two layers are cured, removed from their molds, and their joining faces are dipped in a thin layer of uncured elastomer. (3) Lastly, the two layers are joined and cured together. The primary limitation of this soft lithography fabrication process is that it is fundamentally 2.5D, meaning that the robots are largely constrained to a planar morphology. This process limits a soft robot's ability to achieve amorphous, 3D forms. Additionally, Umedachi et al. [2013] provide the first SMA actuated soft robot fabricated using 3D printing. However, although 3D printing allows printing flexible materials in amorphous forms, these materials are relatively brittle with respect to casted rubbers and are not well-suited for FEAs.

2.3.1 Soft Locomotory Robots

In the past several years soft roboticists have made many notable low durometer rubber robots intended for land and water locomotion. For example, rolling belts have been produced by Correll et al. [2010] and Marchese et al. [2011]. Trimmer et al. [2006] and Umedachi et al. [2013] emulated the peristaltic locomotion of caterpillars. Shepherd et al. [2011] developed a multigait walking robot, and Shepherd et al. [2013a] developed a jumping robot powered by combustion. However, a limitation of the aforementioned locomotory robots is that they require an electrical and/or pneumatic tether. Soft

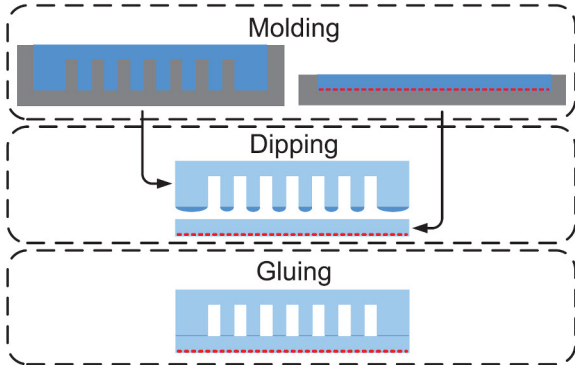


Figure 3: Soft lithography fabrication process for soft fluidic elastomer robots. Reproduced with permission from Onal and Rus [2012].

actuation systems, especially fluidic actuation systems, typically require significant supporting hardware and often limit soft locomotory robots from being self-contained. That said, there are a few examples of untethered soft robots: Onal et al. [2011] created a rolling robot, Onal and Rus [2013] emulated the serpentine locomotion of snakes, and Tolley et al. [2014b] developed a quadrupedal walking robot; these are all soft-bodied fluidic elastomer systems. Seok et al. [2010] realize peristaltic locomotion with a self-contained SMA-based inchworm. However, a limitation of all these untethered soft platforms is that performance is severely limited with respect to their rigid-bodied counterparts, and this limitation is due to the constraints imposed by bringing onboard all supporting hardware. More specifically, they all exhibit locomotory speeds of between 0.008 and 0.07 bodylengths per second. Recently, Marchese et al. [2014c] developed an autonomous soft robotic fish that can swim at speeds of 0.4 body lengths per second.

2.3.2 Soft Continuum Manipulators

Recently, continuum manipulators composed from soft elastic material have been developed. These soft rubber manipulators can be categorized under two primary morphologies. First, there are tendon driven manipulators consisting of variable length tendons, typically cables or shape memory alloy wire (see Section 2.1.1), embedded within and anchored to portions of a soft silicone arm. For example, previous work on soft bio-inspired octopus-like arms developed by Calisti et al. [2010] used tendons and demonstrated capabilities like grasping and locomotion [Laschi et al., 2012, Calisti et al., 2011]. Also, Wang et al. [2013] developed a cable driven soft rubber arm consisting of one large actuated segment that bends bi-directionally. Lastly, McEvoy and Correll [2014a] and McEvoy and Correll [2014b] used a programmable stiffness spine in conjunction with tendons to achieve shape change in a soft rubber arm. The second morphology uses fluidic elastomer actuators (see Section 2.1.3) distributed among the manipulator’s soft body segments. The primary advantages of using fluidic actuation for soft continuum manipulators is that this energy transmission system: (i) can be lightweight making

for easy integration into distal locations of the body, (ii) conforms to the time varying shape of the manipulator, and (iii) does not require rigid components to implement. There are several examples of soft fluidic grippers described in recent literature. Deimel and Brock [2013] developed a pneumatically actuated three-fingered hand made of fiber reinforced silicone that is mounted to a hard industrial robot and capable of robust grasping. More recently, they have used similar fiber reinforced actuation technology to develop an anthropomorphic soft pneumatic hand capable of dexterous grasps [Deimel and Brock, 2014]. Additionally, we have previously shown planar manipulation is possible with an entirely soft robot. That is, a six-segment planar fluidic elastomer robot can be precisely positioned using a closed-loop kinematic controller [Marchese et al., 2014b,a, Katzschmann et al., 2015]. Ilievski et al. [2011] created a pneumatic starfish-like gripper composed of FEAs and demonstrated it grasping an egg. Stokes et al. [2014] used an FEA-based elastomer quadrupedal robot to grasp objects in a hard-soft hybrid robotic platform. A puncture resistant soft pneumatic gripper is developed in Shepherd et al. [2013b]. An alternative to positive pressure actuated soft grippers is the robotic gripper based on the jamming of granular material developed in Brown et al. [2010]. Another relevant piece of work is the manually operated 3D elastomer tentacles developed by Martinez et al. [2013] containing 9 pneumatic crescent-shaped channels embedded within 3 body segments.

3 Actuators

In this section we detail the design and fabrication of three different soft fluidic elastomer body segments. Each type of body segment can serve as a unit-module for composing different soft robot body morphologies. The primary design constraint is that the actuated body segments should be composed almost entirely from soft materials. The primary functional specification is that these actuated segments should integrate into an autonomous robotic systems. That is, they should be capable of performing tasks such as trajectory-following in free space, moving dexterously through confined spaces, and/or grasping and placing objects, all without human intervention.

3.1 Operating Principles

Despite the variability in fluidic elastomer actuator morphologies, their fundamental operating principles are universal. This section provides an overview of these operating principles. Generally, each segment of a fluidic elastomer bends and this bending is due to material strain. Figure 4 illustrates how unidirectional bending arises from material strain. Consider a block of elastomer where the edges of the top and bottom surfaces have equal lengths, L_0 . If the top surface is strained such that its new edge length is $L_0 + \Delta L$, but the bottom of this block remains unextended, then the elastomer will bend. Bending is the basic motion primitive of the fluidic elastomer robot.

In order to generate strain within the elastomer, this class of

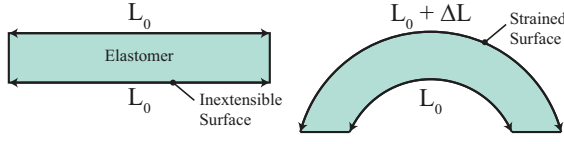


Figure 4: Operating principle of a bending elastomer segment. One surface of the elastomer is strained while the opposite side remains unextended. The difference in length produces bending.

actuator uses pressurized fluids. Essentially, expandable, fluid-filled chambers are embedded within the elastomer. When these chambers are pressurized, the entrapped fluid generates stress in the material causing the material to strain. This concept is illustrated in Figure 5A and Figure 5B. Here, the entrapped fluid is shown in yellow and its pressure is p_c . In order to express the relationship between fluid pressure and elastomer deformation, we can use a one-dimensional simplification of an iterative model presented in Marchese and Rus [2015]. Let \bar{h} and \bar{t} be the initial undeformed diameter and wall thickness of a cylindrical elastomer channel, and let \hat{h} and \hat{t} represent the deformed diameter and wall thickness. Algorithm 1 expresses how the channel's diameter grows as a function of pressure. Stresses are successively updated based on deformed channel dimensions. Here, Δp_c is a vector of all consecutive incremental pressure increases until the maximum channel pressure p_c^{\max} is reached. The stress and strain in the elastomer are represented by σ and ϵ , respectively. The procedure `strainLookUp()` provides a nonlinear mapping from stress to strain.

Algorithm 1: Iterative Channel Deformation

```

Input:  $\bar{t}$ ,  $\bar{h}$ ,  $\Delta p_c$ ,  $p_c^{\max}$ 
 $\hat{h} \leftarrow \bar{h}$ .
 $\hat{t} \leftarrow \bar{t}$ .
 $\bar{c} \leftarrow \pi \left( \frac{\bar{t}}{2} + \bar{h} + \frac{\bar{t}}{2} \right)$ .
 $p_c \leftarrow P_{\text{atm}}$ .
 $i \leftarrow 0$ .
repeat
   $\sigma \leftarrow p_c \frac{\hat{h}}{2\hat{t}}$ .
   $\epsilon \leftarrow \text{strainLookUp}(\sigma)$ .
   $\hat{c} \leftarrow \bar{c}(1 + \epsilon)$ .
   $\hat{h}, \hat{t} \leftarrow \text{solve} \left\{ \begin{array}{l} \text{Circumferential Strain:} \\ \hat{h} = \frac{\hat{c}}{\pi} - \hat{t} \\ \text{Conservation of Material Volume:} \\ \pi \left[ \left( \frac{\hat{h}}{2} + \hat{t} \right)^2 - \frac{\bar{h}^2}{4} \right] = \pi \left[ \left( \frac{\bar{h}}{2} + \bar{t} \right)^2 - \frac{\bar{h}^2}{4} \right] \end{array} \right\}$ .
   $p_c \leftarrow p_c + \Delta p_{c,i}$ .
   $i++$ .
until  $p_c \geq p_c^{\max}$ 

```

3.2 Actuator Morphologies

This section provides an in-depth look at three separate soft elastomer body segments actuated using pressurized fluids. We use a defining structural feature to refer to each of the presented segment morphologies, those are (i) ribbed, (ii) cylind-

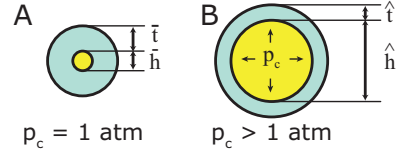


Figure 5: Operative principle of producing material strain through fluidic power. (A) Fluid, shown in yellow, is entrapped in an elastomer channel. (B) When the fluid is pressurized, stress and therefore strain are generated in the material.

drical, and (iii) pleated. In Section 7, these segments are combined serially to form multi-body manipulators and in Section 6 they are used to form single and multi-body locomotory robots. Although similar in material composition and function, differences in internal and external structure and form lead to several distinct difference between the three presented morphologies. First, we present each morphology, examining the structural differences. Then, we provide a comparative characterization of the segments, highlighting salient performance characteristics.

3.2.1 Ribbed Segment

The ribbed fluidic elastomer actuator with its multiple rectangular channels was first implemented and characterized in Correll et al. [2010] followed by Onal et al. [2011], Onal and Rus [2013]. Joining two fluidic elastomer actuators in an agonist-antagonist pairing provides bidirectional bending. This actuator type provided the fundamental segment-level structure of the manipulator developed in Marchese et al. [2014b]. We refer to this three layer composite here as a ribbed segment. That is, two actuator layers are combined in a pair, but separated by an inextensible constraint layer. An implementation of this segment morphology is shown in both a neutral (Fig. 6A) and bent state (Fig. 6B). Bending is produced through the pressurization of agonist fluidic channels (Fig. 6b) that are embedded within the actuated layers (Fig. 6, layers 1 and 3). The structure of the actuated layers is cast from soft elastomer (Fig. 6a). When pressurized, the agonist fluidic channels expand and strain the elastomer. This deformation is transferred into bending by means of an inextensible but flexible constraint (Fig. 6c) embedded within the center layer (Fig. 6, layer 2). Ribs located between channels (Fig. 6e) mitigate strain normal to the inextensible neutral axis. At the segment level, Marchese et al. [2014b] extended the ribbed segment design to make it suitable for inclusion in a multi-segment manipulator. Specifically, fluidic supply channels (Fig. 6d) were introduced on either side of the inextensible constraint and embedded within the center layer. Each segment accommodates multiple, parallel supply channels, two for each body segment within the manipulator. For a detailed model of how a ribbed segment deforms under fluidic pressure input, please refer to Marchese et al. [2014c]. It is important to note that this simplifying static model assumes that ribbed channels deform purely by extending their side and top walls, and that these wall stresses are based on initial channel geometry. In reality, as is shown here in Al-

gorithm 1, wall stresses change as a function of the deformed geometry. If needed, Algorithm 1 can be used to augment the ribbed model used for the soft robotic fish in Marchese et al. [2014c].

Pros: The primary benefits of this morphology in relation to alternatives presented in this section are: (1) Ribs between channels mitigate strain normal to the neutral axis. (2) For a fixed fluid energy input, this segment exhibits greater bending than the cylindrical segment.

Cons: The primary disadvantages of this morphology in relation to alternatives presented in this section are: (1) The three layer structure is prone to delamination and rupture under high strain. (2) Manufacturing this rectangular, layered structure is challenging because all transmission lines must be embedded within the thin constraint layer.

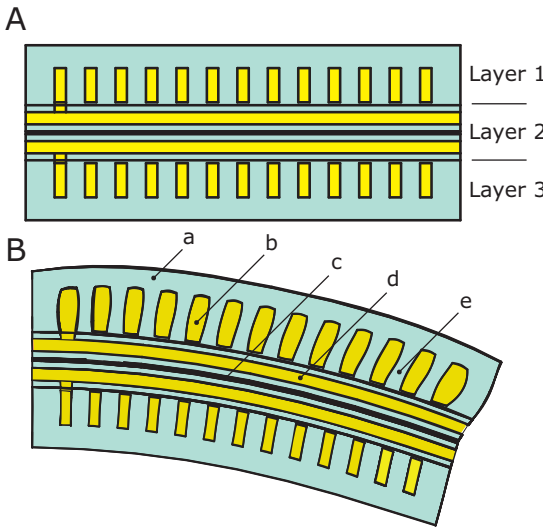


Figure 6: A conceptual representation of the ribbed segment morphology. The segment is composed of three layers produced from soft elastomer (a), embedded fluidic channels (b), inextensible, but flexible constraint (c), embedded fluid transmission lines (d), and ribbed structures (e). (A) The segment in an unactuated, or neutral state. (B) The segment in an actuated state where fluid within the agonist channel group is pressurized producing bending about the inextensible axis.

3.2.2 Cylindrical Segment

The cylindrical fluidic elastomer segment is an alternative to the ribbed design. This design was first presented by the authors in Marchese et al. [2014a]. Design inspiration was drawn from the soft rubber tentacles developed by Martinez et al. [2013] which use embedded crescent-shaped channels in a similar two-layer rubber construction. Although the cylindrical segment morphology is notably different from the ribbed segment, the fundamental operating principles are the same. In the cylindrical morphology (Fig. 7A and B), we transition from a rectangular, planar-layered composite to a cylindrical, concentric-layered composite. Specifically, the segment consists of three concentric layers: (i) an outer soft layer

(Fig. 7b, transparent), (ii) a slightly stiffer inner layer (Fig. 7d, green), and (iii) a hollow core that accommodates a bundle of fluid transmission lines (Fig. 7f, white). Two fluid-filled, and cylindrically-shaped channels are embedded laterally within the outermost layer (Fig. 7c). These channels interface with the transmission lines by means of a stiffer rubber inlet piece (Fig. 7a, brown). When pressurized, the entrapped fluid deforms the embedded channel both circumferentially and longitudinally (Fig. 7B). Specific to this morphology, the inner tube-like layer composed of slightly stiffer rubber serves as an inextensible constraint, transforming channel deformation into segment bending.

Pros: The primary benefits of this morphology in relation to alternatives presented in this section are: (1) Entirely composed of rubber, the resiliency and the durability of the actuator are increased. (2) The two cylindrical channels make this segment the simplest to fabricate. (3) Embedded fluidic channels are not at the interface between fabricated layers, making this morphology robust against delamination under high pressures.

Cons: The primary disadvantages of this morphology in relation to alternatives presented in this section are: (1) The simple channel design exhibits high circumferential strain. Compared to the ribbed and pleated morphologies, more fluid energy is required to produce bending. (2) When the segment bends, an increased volume of rubber on the antagonist side of the actuator has to be compressed. This inhibits a high maximum curvature.

3.2.3 Pleated Segment

The pleated channel design is detailed in Figure 8 and consists of evenly spaced, discrete elastomer sections (Fig. 8d), which are separated by gaps (Fig. 8c). Embedded within each elastomer section is a hollow channel (Fig. 8e). Cut views of the un-actuated and actuated states are shown in Figure 8A and Figure 8B, respectively. This design approach draws inspiration for its pleats from the soft pneumatic gloves developed by Polygerinos et al. [2013] and its homogeneous body design is inspired from the tail design of a soft robotic fish developed by Katzschmann et al. [2014]. The hollow channels within each pleat are connected via a center channel and are accessible through a front inlet (Fig. 8a). When fluid within these channels is pressurized (Fig. 8, yellow), an individual pleat undergoes a balloon-like expansion of the thin exterior skin both normal and parallel to the neutral axis. Similar to the cylindrical actuator design, a stiffer silicone layer (Fig. 8, blue) serves as an almost inextensible constraint layer. The sum of the balloon-like expanding motions leads to bending of the less extensible center constraint layer.

Pros: The primary benefits of this morphology in relation to alternatives presented in this section are: (1) A unidirectional pleated actuator is capable of bending to higher curvatures than the ribbed or cylindrical morphology. (2) A bidirectional pleated segment is capable of exerting higher maximum forces because of its ability to accommodate the largest energy input. (3) Using a lost-wax casting approach, the cyan portion

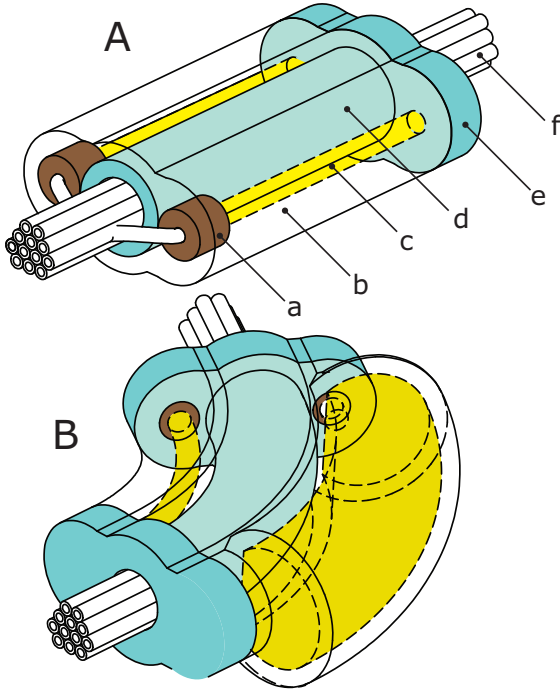


Figure 7: A conceptual representation of the cylindrical segment morphology. The segment consists of a soft silicone rubber outer layer (b, transparent), a slightly stiffer silicone inner layer (d, cyan), crush resistant silicone inlets (a, brown), expanding embedded fluidic channels (c, yellow), and an internal tubing bundle (f, white). The segment terminates in soft endplates (e). (A) A depiction of the segment in an unactuated state. (B) A depiction of the body segment in an actuated state where the expansion of the pressurized fluidic channel is schematically represented.

of this segment can be cured in a single step, avoiding seams that are prone to delamination.

Cons: The primary disadvantages of this morphology in relation to alternatives presented in this section are: (1) The morphology is more complex to manufacture because it requires a lost-wax casting procedure detailed in Section 4.3. (2) The implementation of this morphology requires the most fluid energy to actuate it to appreciable tip forces. This might very well be due to the fact that, when compared to the other implementations, this implementation is larger in size and uses a higher shore hardness elastomer.

3.2.4 Comparative Characterization

To characterize the actuated segments, we first perform bending tests to experimentally determine the relationship between the segment's neutral axis bend angle θ , internal channel pressure p_c , and supplied volume V_s for each morphology. In these experiments, the base of each segment is grounded securely in a fixture and the segment's tip is supported vertically with a ball transfer. Then, the segment's agonist channel is incrementally filled under closed-loop volume control via the displacement of a fluidic drive cylinder; please refer to Sec-

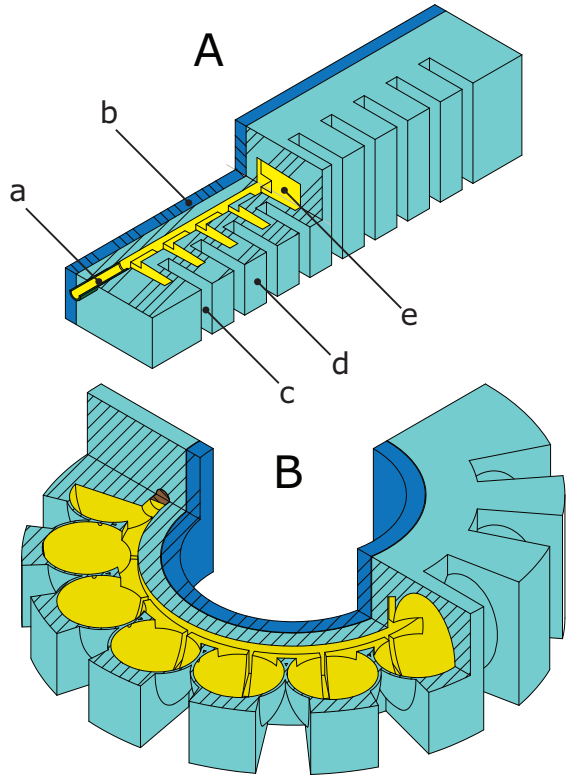


Figure 8: A conceptual representation of the pleated segment morphology. The design consists of a channel inlet (a), an almost inextensible constraint layer (b), uniform pleats (d) separated by even gaps (c), and internal channels within each pleat (e). (A) depicts the segment in an unactuated state and (B) shows the segment in an actuated and therefore bent state. The expansion of the pressurized channels are schematically represented.

tion 5. After each incremental fill, we allow pressure within the cylinder and within the actuated channel to equalize before measurements of the channel's pressure and the segment's curvature are taken. Curvature is assumed to be constant along the length of the segment and is uniquely defined by measuring the cartesian locations of the base and the tip of the segment; refer to Marchese et al. [2014b]. From this curvature we compute the segment's bend angle. Since this is a quasi-static process, fluid pressure and supply volume measurements can be used to determine the elastic potential fluid energy input into the actuation system, which consists of the elastomer segment and the internal compressible transmission fluid. The potential energy is calculated by

$$V_{Elastic} = \int_0^{V_c} p_c(V) dV. \quad (1)$$

Additionally, a blocking force test is performed in order to understand the variability in tip force output between segment morphologies. Again, a similar experimental procedure is used as for the bending characterization; however, during blocking force experiments a plate attached via a force transducer to ground is mounted in contact with the segment's tip,

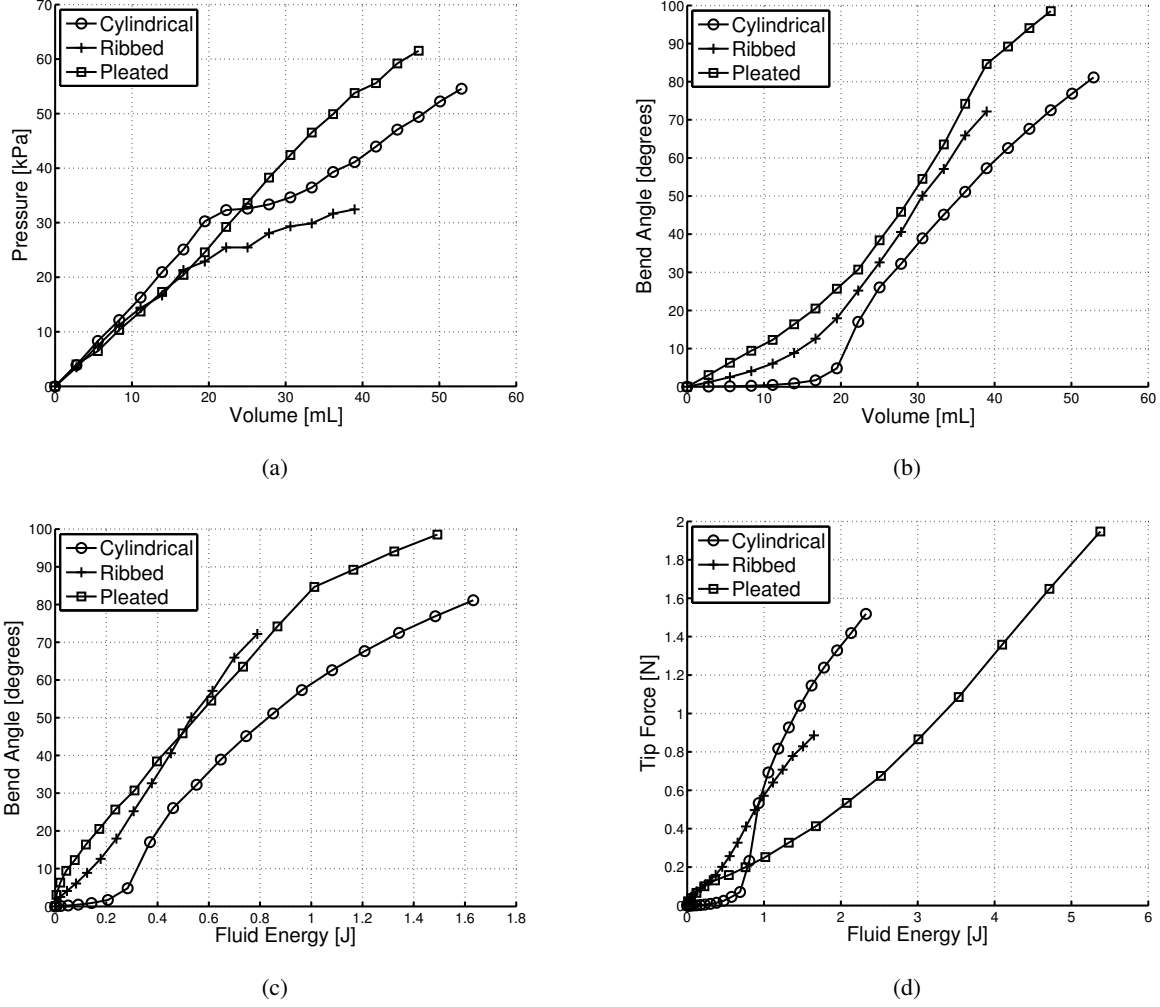


Figure 9: Experimental characterizations of three actuated segment morphologies performed by filling each actuator by means of controlled volumetric displacements and measuring internal pressure, neutral axis bend angle under a constant-curvature assumption, and blocking force.

orthogonal to the bending plane. This effectively measures the force required to block the actuator from bending.

Figure 9 details the results of these characterization experiments from which we can make several observations. First, the pleated morphology is generally the stiffest, followed by the cylindrical, and then the ribbed, where stiffness is defined as $\frac{\partial p_c}{\partial V_c}$ (Fig. 9a). Second, the cylindrical morphology has a salient bend angle nonlinearity (Fig. 9b). More specifically, small volumetric fluid changes of less than 15 mL provide little control authority over curvature; however, above 25 mL displacements, the control authority is strong and the curvature-volume relationship is approximately linear. Third, the cylindrical morphology requires the most amount of fluid energy to produce a given bend angle and the ribbed and pleated segments require approximately the same amount of fluid energy to generate equivalent bending (Fig. 9c). Lastly, the pleated segment generally requires more fluid energy than both the ribbed and cylindrical morphologies to produce a given tip force. However, the pleated segment can accommodate sig-

nificantly higher input energies and therefore can reach the highest maximum tip force.

4 Fabrication

Three distinct fabrication techniques for soft actuators are presented in this section. Table 1 contains the superscript references to machine tools and materials used.

4.1 Lamination Casting with Heterogenous Embeddings

Lamination-based casting with heterogeneous embeddings is a fabrication technique that extends current soft lithography casting processes. As detailed in Section 2.3 and in Figure 3, the outer layers of a soft robot are often cast separately using soft lithography techniques to inlay channel structures. Then, these layers are laminated together with a constraint layer to

form the actuator. To power actuation, supply lines are pierced through the actuator's side wall and run external to the mechanism. This approach can be prohibitive in that it creates an unreliable pneumatic interface between supply lines and actuated channels and also these external supply lines can inhibit the robot's movement or otherwise obstruct it from completing its intended function. By embedding heterogeneous components within the elastomer layers as they are cast, we address both of these challenges. In this section, we show how the idea of soft lithography can be combined with embedding heterogeneous components and that it is well-suited for realizing the ribbed body segment morphology. Specifically, we illustrate this fabrication process in the context of creating both a soft ribbed manipulator and soft ribbed fish robot.

A ribbed manipulator, like that detailed in Section 7.1, can be fabricated using lamination-based casting with heterogeneous embeddings. The specific approach for fabricating a six segment manipulator is illustrated in Figure 10. Here, seven constraint supports (Fig. 10d) are 3D printed¹ and placed into a constraint layer mold (Fig. 10f), which is also 3D printed. The constraint film (Fig. 10c) is cut from a thin acetal sheet⁸ using a laser² and inserted through the aforementioned supports. Above and below the constraint film, eight pieces of silicone tubing (Fig. 10a) are threaded through the supports. Silicone rubber³ is then mixed and poured into the constraint layer mold, immersing tubing, film, and supports in a layer of elastomer to create the composite constraint layer (Fig. 10g). The uncured rubber inside the mold is then immediately degassed using a vacuum chamber⁴. Once cured, small holes are created in the constraint layer to pierce the embedded tubing at specific locations, allowing each line to independently address a group of fluidic channels. Elastomer pieces containing channels (Fig. 10b) are casted and cured separately using a similar molding technique. Those cured elastomer pieces (Fig. 10b) are then carefully attached to both faces of the constraint layer using a thin layer of silicone rubber. Lastly, the printed feet (Fig. 10e) are attached to the constraint supports (Fig. 10d) to create an attachment point for ball transfers (Fig. 18ad). These mechanisms help constrain the arm's motion to a plane.

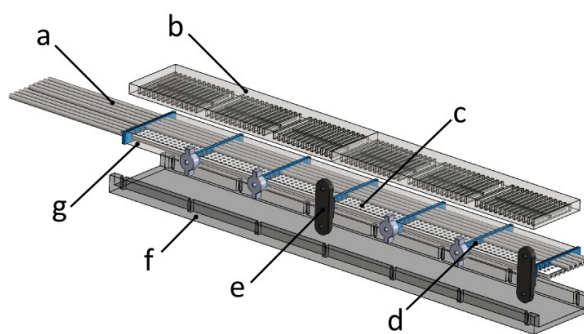


Figure 10: Fabrication process for a ribbed manipulator: silicone tubing (a), elastomer pieces containing channels (b), constraint film (c), constraint supports (d), feet (e), constraint layer mold (f), and composite constraint layer (g).

The anatomically proportioned body of a fish-like robot developed by the authors in Marchese et al. [2014c] and detailed in Section 6.1 was also fabricated using a similar lamination-based casting process, and this process is detailed in Figure 11. Supply lines that connect the posterior actuator pair are embedded within the body during step 2 (Fig. 11-2).

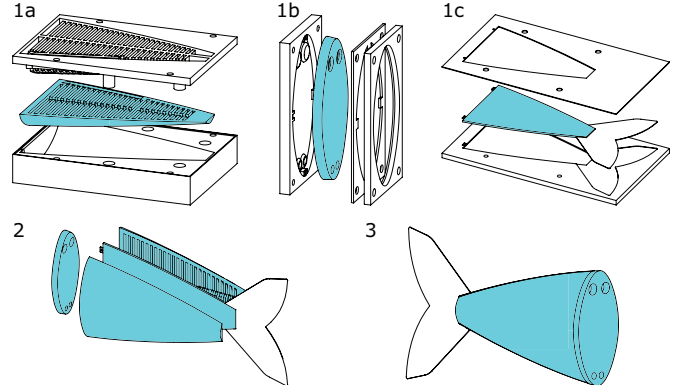


Figure 11: Illustration of the soft fish body fabrication process. First, two halves of the body (1a), a connector piece (1b), and a constraining layer (1c) are all cast from silicone using two-part molds. Next, these four pieces are sequentially bonded together using a thin layer of silicone (2). Lastly, once cured the fish body is ready for operation (3). This figure and caption are reproduced with permission from Marchese et al. [2014c].

4.2 Retractable Pin Casting

Retractable pin casting allows the relatively simple channel structure of the cylindrical body segment to be cast without lamination. This fabrication process is advantageous because it eliminates the rupture-prone seems between the channels and constraint layer seen in the ribbed morphology fabricated through lamination-based casting. Additionally, retractable pin casting is well-suited for the modular fabrication of multi-body soft robots. Here, segments are individually cast and then concatenated together to form the robot. Specifically, in this section we demonstrate retractable pin casting in the context of fabricating a cylindrical manipulator.

A cylindrical manipulator, like that detailed in Section 7.2, is fabricated through a retractable-pin casting using pourable silicone rubber^{3,5} and 3D printed molds¹. Figure 12 details this process. First, each body segment is independently fabricated in steps 1-3 and later these segments are joined serially to form the arm in steps 4 and 5. To start, a four piece mold is printed. The mold is then poured in two steps. In step 1, a low elastic modulus rubber³ is mixed, degassed in a vacuum⁴, and poured to form the body segment's soft outer layer shown in white. The mold's outer piece, one half of it is shown in green, functions to form the segment's exterior. Metal rods shown in pink are inserted into the mold and are held in place by the orange bottom piece of the mold. These rods will form the cavities for the segment's two lateral fluidic actuation channels. After the outer layer has cured, the red rigid sleeve is removed

in step 2 from the extruded feature of the *orange* bottom piece of the mold. This produces a cavity into which a slightly stiffer rubber⁵ is poured, forming the segment's partially constraining inner layer shown in *cyan*. The extruded feature of the *orange* bottom piece, shown by its *orange* end tip, functions to produce the segment's hollow interior core. In step 3, the body segments are removed from their molds and joined to rubber⁵ endplates shown in *cyan* using silicone adhesive⁶. The small *yellow* channel inlets were added on one side of the *pink* metal pins during step 1. In step 4, soft silicone tubes⁷ are joined to each embedded channel's inlet. The resulting bundle of tubes is passed through each segment's hollow interior. Lastly, in step 5 multiple body segments are attached at their endplates using the same adhesive⁶.

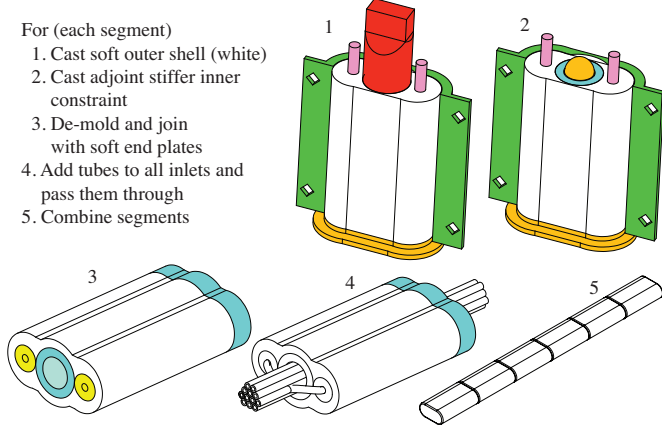


Figure 12: Fabrication process for the cylindrical manipulator morphology: Each body segment is casted using a two step process where the outer soft layer (1) and inner stiffer layer (2) are poured. Once cured, the segments are joined to endplates using silicone adhesive (3). Next, silicone tubing is connected to each embedded channel and the resulting tubing bundle is run inside each segment's hollow interior (4). Lastly, the body segments are serially connected using adhesive to form the manipulator (5).

4.3 Lost Wax Casting

As mentioned, existing soft robots are often produced through a multi-step lamination process, which produces seams and is prone to delamination. By abandoning the need for lamination, the retractable pin fabrication process enables seamless channel structures; however, the channel structures are limited to a relatively simple shape. For these reasons, we introduce lost-wax casting as part of the fabrication process for soft actuators. With this, arbitrarily shaped internal channels can be achieved to enable a wider range of applications. As examples, in this section we fabricate a pleated uni-directional gripper and a ribbed soft fish tail using the lost-wax approach.

The complete fabrication process for a pleated actuator consists of eight steps that are depicted in Figure 13. In step (A), harder silicone rubber¹⁰ is poured into a mold, which contains a 3D printed model of the wax core. In preparation for step

(B), the model is removed and the rubber mold is left inside the outer mold. Next, a rigid rod or tube, for example made of carbon fiber¹², is used as a supportive inlay for the wax core. The rod is laid into the cavity of the rubber mold, supported on both ends by the outer mold. This ensures that the wax core does not break when removed from the rubber mold. Mold release spray is applied to the silicone rubber mold to ease the wax core removal process. The wax¹¹ is heated up until it becomes fully liquefied. The assembly of the rubber mold and the outer mold is heated up for a few minutes to the same temperature as the wax. Using a syringe, the liquid wax is injected into the assembly. Within a few minutes, the injected wax will start to solidify and significantly shrink in volume; this is counteracted by injecting more hot wax into the solidifying wax core during the cool down period. In step (B), the wax core is first allowed to completely cool down, then it is released from the mold. In step (C), the cooled down wax core is assembled together with the bottom mold, which defines the pleated structure of the actuator. The mold assembly is aligned with a top mold using pins. This top mold provides additional volume to cover the wax core. In step (D), low elastic modulus rubber³ is mixed, degassed in a vacuum⁴, and poured to form the pleats and allowed to cure. In step (E), stiffer rubber is poured on top of the cured pleats to form a constraint layer. In step (F), the cured actuator is removed from the mold. In step (G), most of the wax core is melted out by placing the cured actuator into an oven in an upright position. After this, remaining wax residues are cooked out in a boiling water bath. Finally, in step (H) a silicone tube⁹ and a piece of silicone cord¹³ get covered with silicone adhesive⁶ and are inserted into the front and back holes, respectively. The actuator can be used as a unidirectional gripper (see Figure 7) or as one agonist actuated segment within a multiple body manipulator (see Section 7.3).

The actuated body of the hydraulic fish detailed in Section 6.2 is also produced via lost-wax casting. The fabrication process is depicted in Figure 14. In step (A), the rubber mold is poured and cured inside an assembly consisting of an outer mold with lid and a model for the core inside of it. In preparation for step (B), the lid and the model core are removed and the rubber mold is left inside the outer mold. The rubber mold receives a small carbon fiber tube as an inlay in its center cavity. This ensures that the wax core does not break when being removed from the rubber mold. Mold release spray is applied to the silicone rubber mold to ease the wax core removal process. The wax is heated up until it becomes fully liquefied. The assembly of rubber mold and outer mold is heated up for a few minutes to the same temperature as the wax. Using a syringe, the liquid wax is injected into the assembly. Within a few minutes, the injected wax will start to solidify and significantly shrink in volume; this is counteracted by injecting more hot wax into the solidifying wax core during the cool down. In step (B), the wax core is first allowed to completely cool down, then it is released from the mold. In step (C), a head constraint, a center constraint, and two wax cores are assembled together inside the tail mold halves using spacers, positioning pins and screws. In step (D), a mix of silicone rubber with glass bub-

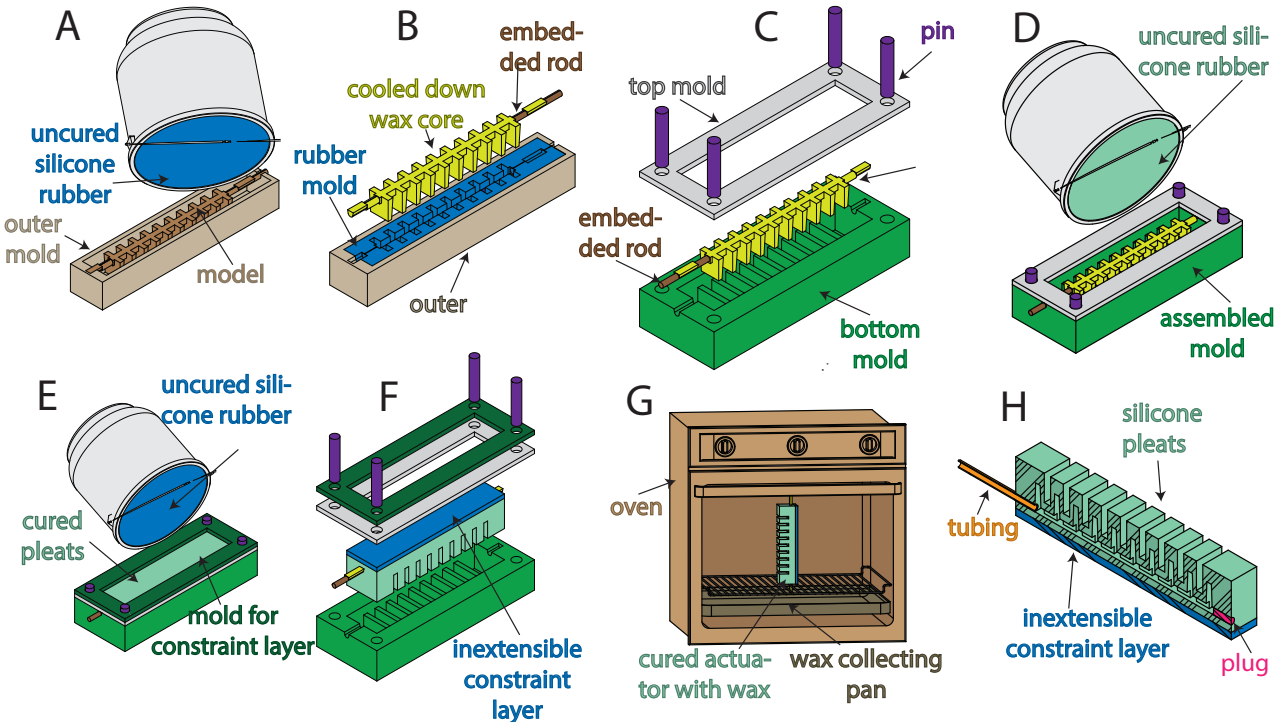


Figure 13: Fabrication process for the pleated actuator morphology: (A) Pour and cure a rubber mold, (B) pour wax core with embedded supportive rod, (C) combine bottom mold, top mold and wax core using pins, (D) pour rubber into assembled mold, (E) pour stiffer rubber on top of the cured actuator to form a constraint layer, (F) remove cured actuator from mold, (G) melt out wax core from the actuator using an oven, and (H) add silicone tubing and plug using silicone sealant.

bles is poured into the tail assembly and allowed to cure. In step (E), most of the wax core is melted out by placing the fish tail in an upright position into an oven. Finally, in step (F) the remaining wax residues are cooked out in a boiling water bath.

Table 1: Commercially Available Tools and Equipment

#	Product Name	Company
1	Fortus 400mc	Stratasys
2	VLS3.50	Universal Laser Systems
3	Ecoflex 0030	Smooth-On
4	AL Cube	Abbess Instr. & Systems
5	Mold Star 15	Smooth-On
6	Silicone Sealant 732	Dow Corning
7	PN 51845K52	McMaster
8	PN 5742T51	McMaster
9	PN 51845K53	McMaster
10	Mold Star 30	Smooth-On
11	Beeswax	Jacquard
12	PN 2153T31	McMaster
13	PN 9808K21	McMaster

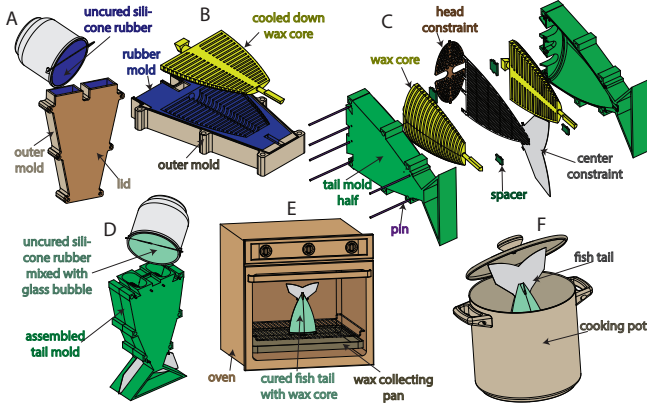


Figure 14: Fish tail fabrication process: (A) Pour and cure a rubber mold, (B) pour wax cores, (C) combine head constraint, center constraint and wax cores with tail mold halves, (D) pour rubber mixed with glass bubbles into assembled tail mold, (E) using an oven melt out wax core from the cured fish tail, and (F) cook out remaining wax to create desired actuator cavities.

5 Power

Fluidic power sources present many challenges for soft robots. There are three major ways to characterize these power sources: by transmission fluid, circuit continuity, and portability.

5.1 Transmission Fluids

Recently, Wehner et al. reviewed existing pneumatic energy sources. However, in general the actuators detailed in Section 3.2 can be powered using either pneumatic or hydraulic systems where gases or liquids, respectively, are the transmission fluid. Pneumatics are advantageous for powering FEAs because they provide a low viscosity power transmission medium. High flows can be achieved with relatively low driving pressures. However, gases also introduce compressibility into the power transmission system and these dynamics can be difficult to model (refer to Marchese et al. [2015a]) and can produce undesirable time delays. Hydraulics are advantageous because liquids are relatively incompressible when compared to gases, meaning power can be transferred almost immediately from the power source to the actuators. However, to achieve comparable volumetric flow rates liquid drive systems often require high driving pressures and/or low impedance (large diameter) power transmission lines because of the increased viscosity of the transmission medium.

5.2 Circuit Continuity

Further, the actuators detailed in Section 3.2 can be powered using either open-circuit or closed-circuit power systems. Open-circuit power systems exhaust the transmission fluid to the environment, whereas closed-circuit systems recover fluid delivered to the actuators. Open-circuit systems are advantageous because they do not require mechanisms to re-pressurize

and return transmission fluid to the supply. However, they often rely on passively exhausting transmission fluid to ambient/environmental pressure meaning the actuator depressurization is unactuated and a function of the actuator's compliance and the impedance of the the exhaust pathway. Please refer to Marchese et al. [2011] and Marchese et al. [2014c] for examples of open-circuit power systems. Closed-circuit systems (see Fig. 15) are advantageous because the amount of transmission fluid is constant and moved around within the system; this means the power system's fluid medium is not required to match the operating environment (e.g., a soft robot fish powered by pneumatics swimming underwater). Furthermore, because the volume of transmission fluid is constant the power system can typically vacuum fluid from the actuator under power; meaning the system has control authority over actuator depressurization. The disadvantageous to closed-circuit systems is that they typically require additional plumping to complete the fluid circuit and supporting hardware like a revisable pump. Please refer to Marchese et al. [2014b], Katzschmann et al. [2014] and Marchese and Rus [2015] for examples of closed-circuit power systems.

5.3 Portability

The portability of a power source may be of significant interest to a soft roboticist. For example, locomotory soft robots are typically designed under the constraint of being self-contained, meaning all supporting hardware is located onboard the robot. Additionally, if the untethered robot is intended for high speed maneuvers, then compressed gas [Marchese et al., 2014c] or combustion [Tolley et al., 2014a] are viable power alternatives. However, if prolonged operations are required, then open-circuit pumps [Tolley et al., 2014b, Onal and Rus, 2013] or closed-circuit pumps [Katzschmann et al., 2014] are suitable options.

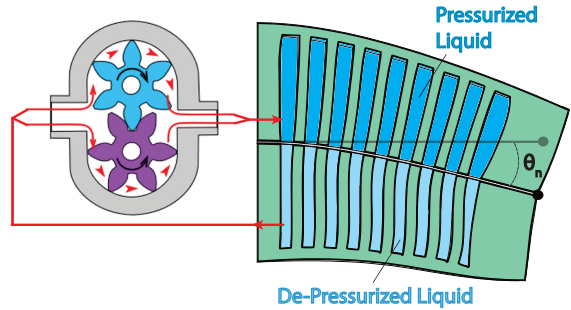


Figure 15: Closed-circuit power system used to drive actuation in the soft hydraulic fish.

6 Locomotion

Soft and continuously deformable locomotion systems can be made from fluidic elastomer body segments. Specifically, in this section we detail how soft robotic fish can be composed

by combining the actuated segments that were presented in Section 3.2 with a portable power system.

6.1 Pneumatic Fish

The soft pneumatic fish developed in Marchese et al. [2014c] with a ribbed actuator is shown as a complete system in Figure 16a and performing an escape response in Figure 16b.

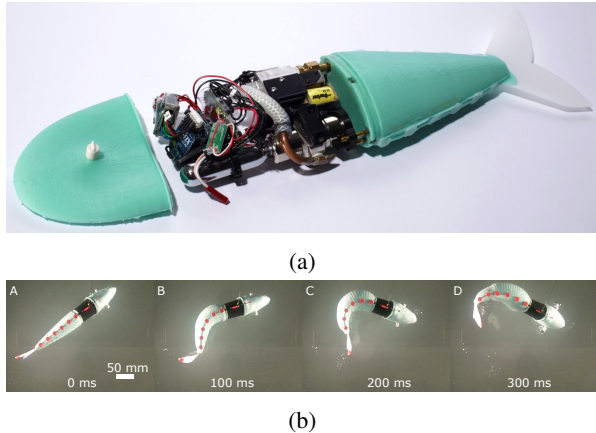


Figure 16: A soft pneumatic robotic fish: (a) An overview of the robotic system, photo courtesy of Devon Jarvis, (b) A sequence depicting the fish performing an escape response.

6.2 Hydraulic Fish

The soft hydraulic fish Katzschmann et al. [2014] with a single ribbed actuator is shown as a complete system in Figure 17a. A close-up view is shown in Figure 17b and the 3d swimming capabilities are shown in Figure 17c.

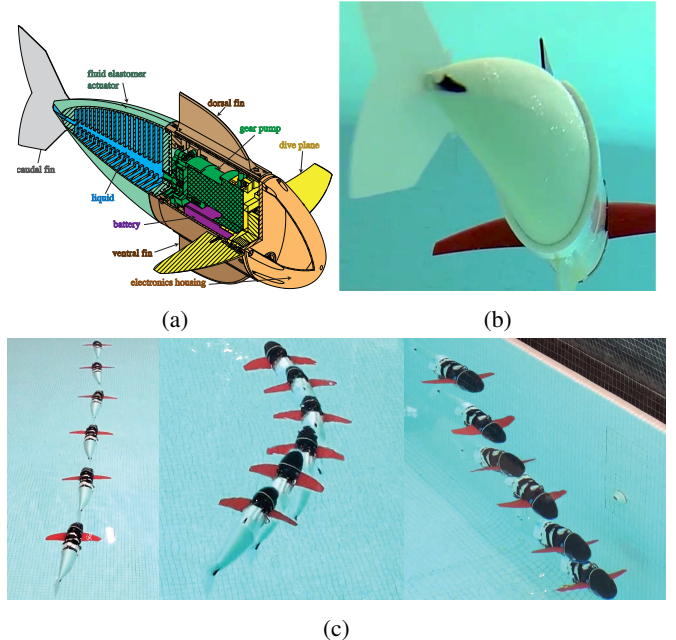


Figure 17: A soft hydraulic robotic fish: (a) A schematic of the system, (b) underwater swimming motion, and (c) example of continuous forward swimming, yaw motion, and diving.

7 Manipulators

Soft and continuously deformable manipulators can be assembled from bending fluidic elastomer segments. Specifically, in this section we detail how multi-segment manipulators can be composed by serially concatenating the actuated segments that were presented in Section 3.2.

7.1 Ribbed

Structurally, a ribbed arm is composed of serially concatenated, homogeneous ribbed body segments. By volume, over ninety-seven percent of the ribbed manipulator is soft silicone rubber, excluding the feet. This manipulator is depicted in Figure 18a and was initially developed in Marchese et al. [2014b]. The manipulator can theoretically be composed of any number of the aforementioned ribbed segments (Fig. 18ae), but practically, we have constructed a six-segment prototype (Fig. 18b). All twelve fluidic transmission lines as well as channel-to-supply interfaces are embedded within the manipulator's center layer. Markers are located at the interface between segments (Fig. 18ab), making segment endpoints identifiable to an external localization system. The starting point of the arm's first segment (Fig. 18aa) is grounded to the platform on which the arm moves and we refer to this as the base. Ball transfers (Fig. 18ad) are also located at each segment endpoint to allow the arm to move on a two-dimensional plane with minimal friction. In many experiments conducted throughout this work, the pose of the arm's end-effector (Fig. 18ac) is controlled.

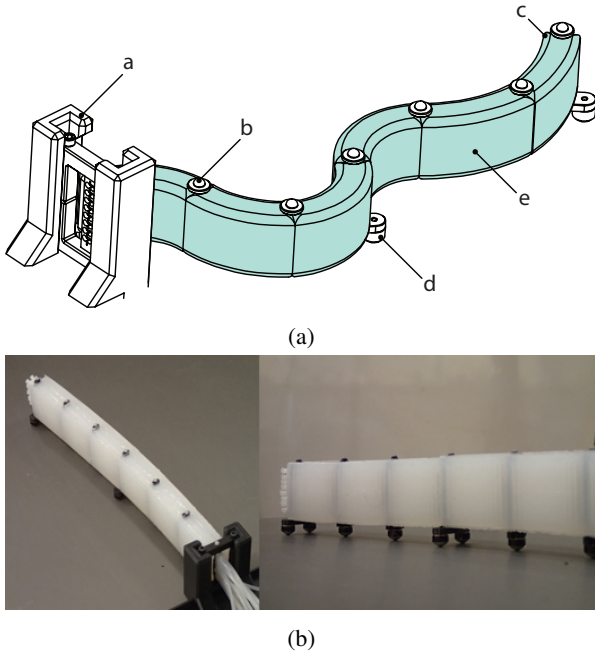


Figure 18: A ribbed soft manipulator prototype. (a) The arm is composed of homogeneous and independently actuated ribbed segments (e). The base of the arm’s first segment is fixed (a) and the end of its last segment is the end-effector (c). Markers (b) identify the endpoints of each segment and ball transfers (d) mitigate friction. (b) Photographs of the ribbed manipulator prototype.

7.2 Cylindrical

We can also compose a manipulator from cylindrical fluidic elastomer segments, as shown in Figure 19 and initially developed in Marchese et al. [2014a]. Just as in the ribbed composition, cylindrical segments are joined end-to-end. Here, fluid transmission lines are passed through the manipulator’s hollow center. This feature not only facilitates segment concatenation, but also allows for modular composition of a manipulator, because transmission lines are not permanently embedded within the elastomer. Additionally, this manipulator type is only composed of soft silicone rubber as there is no inextensible constraint. No other materials are used, except for the attached ball transfers to mitigate ground friction.

Additionally, using four actuated channels per body segment, we have created a multi-segment spatial cylindrical manipulator in Marchese and Rus [2015]. This enables three-dimensional end-effector positioning and is shown in Figure 20.

7.3 Pleated

A manipulator can also be composed from pleated fluidic elastomer segments, as shown in Figure 21. Just as in the ribbed and cylindrical composition, pleated segments are joined end-to-end. The fluid transmission lines are passed through along the central axis of the segments. A supportive hollow profile

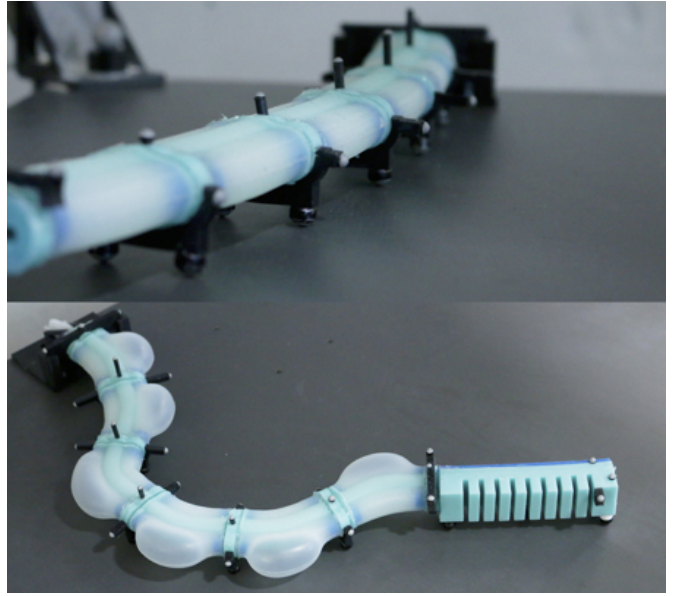


Figure 19: A planar cylindrical soft manipulator prototype with and without a pleated finger-like gripper.



Figure 20: A spatial cylindrical soft manipulator prototype.

can be added to combine two segments. This pleated design allows for modular composition of a manipulator, because transmission lines are not permanently embedded within the elastomer. Additionally, this type of manipulator is, like the cylindrical manipulator, composed entirely of soft silicone rubber.

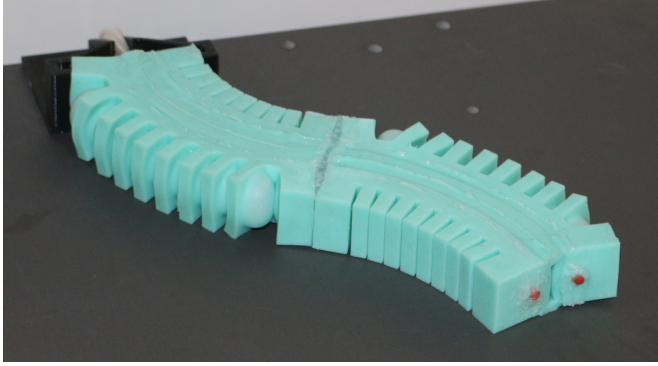


Figure 21: A pleated soft manipulator prototype, composed of two segments with two degrees of freedom each.

8 Discussions

The actuator designs and their fabrication methods described in this paper provide recipes for the rapid fabrication of modular soft robots with arbitrary body morphology.

We showed three fundamentally different fabrication processes and discussed their strengths and weaknesses when using them to build completely soft unit-modules that can be concatenated to multi-segment manipulators or used for locomotion. The lamination and the lost-wax casting processes allow for the embedding of heterogeneous functional elements like constraint layers or tubes into a soft actuator. This facilitates the interfacing to pressure sources or other system components. The simplicity of the retractable pin fabrication method allows for rapid prototyping of simple fluidic elastomer actuators without the risk of failed lamination, and without the need for a wax core. The lost-wax casting allows for almost arbitrarily shaped pressurizable cavity structures, created as a monolithic body without weakening seams caused by a lamination technique.

Furthermore, an experimental characterization of each segment morphology was presented, analyzing and comparing the effects of fluid energy onto a segment’s bend angle and tip force. It was seen that the pleated segment morphology is the stiffest, followed by the cylindrical, and then the ribbed. The cylindrical morphology has a prominent bend angle nonlinearity for low input volumes, but its behavior becomes almost linear for higher inflations. Based on this insight, easier control of this morphology can be achieved through pre-pressureization of a cylindrical segment. Furthermore, the cylindrical morphology requires the most amount of fluid energy to produce a given bend angle. The ribbed and pleated morphology behave very similar in bending. The pleated segment generally requires more fluid energy than both the ribbed and cylindrical morphologies to produce a tip force. However, the pleated segment can accommodate significantly higher input energies and therefore can reach the highest maximum tip force, useful when a more powerful manipulation is required.

This class of completely soft manipulator morphologies is very well-suited for tasks requiring: (i) interactions with humans and environments to be safe, (ii) uncertainty to be miti-

gated at the hardware level, (iii) continuous and dexterous deformation, and/or (iv) hardware to take an unstructured, amorphous form. For example, by making robots from soft elastic materials, with no sharp edges, and with relatively low link inertia, a robot’s reliance on sensors and software for safety is reduced. The prospects for safe integrations between a robot and human are generally increased when the compliance of the material composing the machine match those of soft biological materials Majidi [2014], and this feature is inherent to robots made of soft silicone elastomer. An alternative approach to robot manipulator design is to allow soft segments to handle some uncertainty at the hardware level in order to reduce the burden on the computational system. For example, consider how a soft manipulator passively conforms to the environment’s boundary. A planner is unaware of this complex interaction, but the primary task can still be successfully executed. Further, modern inspection tasks as well as invasive surgery require devices with redundant degrees of freedom and high dexterity and often impose the constraint of navigating around sensitive objects. Soft robotic manipulators may be well-suited for this class of tasks.

References

- Joshua Bishop-Moser, Girish Krishnan, Charles Kim, and Sridhar Kota. Design of soft robotic actuators using fluid-filled fiber-reinforced elastomeric enclosures in parallel combinations. In *Intelligent Robots and Systems (IROS), 2012 IEEE/RSJ International Conference on*, pages 4264–4269. IEEE, 2012.
- Eric Brown, Nicholas Rodenberg, John Amend, Annan Mozeika, Erik Steltz, Mitchell R Zakin, Hod Lipson, and Heinrich M Jaeger. Universal robotic gripper based on the jamming of granular material. *Proceedings of the National Academy of Sciences*, 107(44):18809–18814, 2010.
- Rob Buckingham. Snake arm robots. *Industrial Robot: An International Journal*, 29(3):242–245, 2002.
- M Calisti, A Arienti, ME Giannaccini, M Follador, M Giorelli, M Cianchetti, B Mazzolai, C Laschi, and P Dario. Study and fabrication of bioinspired octopus arm mockups tested on a multipurpose platform. In *Biomedical Robotics and Biomechatronics (BioRob), 2010 3rd IEEE RAS and EMBS International Conference on*, pages 461–466. IEEE, 2010.
- M Calisti, M Giorelli, G Levy, B Mazzolai, B Hochner, C Laschi, and P Dario. An octopus-bioinspired solution to movement and manipulation for soft robots. *Bioinspiration & biomimetics*, 6(3):036002, 2011.
- David B Camarillo, Christopher R Carlson, and J Kenneth Salisbury. Configuration tracking for continuum manipulators with coupled tendon drive. *Robotics, IEEE Transactions on*, 25(4):798–808, 2009.
- Jorge G Cham, Sean A Bailey, Jonathan E Clark, Robert J Full, and Mark R Cutkosky. Fast and robust: Hexapedal

- robots via shape deposition manufacturing. *The International Journal of Robotics Research*, 21(10-11):869–882, 2002.
- Nick Cheney, Robert MacCurdy, Jeff Clune, and Hod Lipson. Unshackling evolution: evolving soft robots with multiple materials and a powerful generative encoding. In *Proceeding of the fifteenth annual conference on Genetic and evolutionary computation conference*, pages 167–174. ACM, 2013.
- Kyu-Jin Cho, Je-Sung Koh, Sangwoo Kim, Won-Shik Chu, Yongtaek Hong, and Sung-Hoon Ahn. Review of manufacturing processes for soft biomimetic robots. *International Journal of Precision Engineering and Manufacturing*, 10(3):171–181, 2009.
- Ching-Ping Chou and Blake Hannaford. Measurement and modeling of mckibben pneumatic artificial muscles. *Robotics and Automation, IEEE Transactions on*, 12(1):90–102, 1996.
- Radoslaw Cieslak and Adam Morecki. Elephant trunk type elastic manipulator-a tool for bulk and liquid materials transportation. *Robotica*, 17(1):11–16, 1999.
- Nikolaus Correll, Cagdas D. Onal, Haiyi Liang, Erik Schoenfeld, and Daniela Rus. Soft autonomous materials - using active elasticity and embedded distributed computation. In *12th Internatoinal Symposium on Experimental Robotics*, New Delhi, India, 2010.
- Frank Daerden and Dirk Lefever. Pneumatic artificial muscles: actuators for robotics and automation. *European journal of mechanical and environmental engineering*, 47(1):11–21, 2002.
- Raphael Deimel and Oliver Brock. A compliant hand based on a novel pneumatic actuator. In *Robotics and Automation (ICRA), 2013 IEEE International Conference on*, pages 2047–2053. IEEE, 2013.
- Raphael Deimel and Oliver Brock. A novel type of compliant, underactuated robotic hand for dexterous grasping. In *Robotics: Science and Systems*, 2014.
- Kevin C Galloway, Panagiotis Polygerinos, Conor J Walsh, and Robert J Wood. Mechanically programmable bend radius for fiber-reinforced soft actuators. In *Advanced Robotics (ICAR), 2013 16th International Conference on*, pages 1–6. IEEE, 2013.
- Ian A Gravagne and Ian D Walker. Uniform regulation of a multi-section continuum manipulator. In *Robotics and Automation, 2002. Proceedings. ICRA'02. IEEE International Conference on*, volume 2, pages 1519–1524. IEEE, 2002.
- Michael W Hannan and Ian D Walker. Kinematics and the implementation of an elephant’s trunk manipulator and other continuum style robots. *Journal of Robotic Systems*, 20(2):45–63, 2003.
- Filip Ilievski, Aaron D Mazzeo, Robert F Shepherd, Xin Chen, and George M Whitesides. Soft robotics for chemists. *Angewandte Chemie*, 123(8):1930–1935, 2011.
- Rongjie Kang, David T Branson, Tianjiang Zheng, Emanuele Guglielmino, and Darwin G Caldwell. Design, modeling and control of a pneumatically actuated manipulator inspired by biological continuum structures. *Bioinspiration & biomimetics*, 8(3):036008, 2013.
- Robert K Katzschmann, Andrew D Marchese, and Daniela Rus. Hydraulic autonomous soft robotic fish for 3d swimming. In *International Symposium on Experimental Robotics (ISER)*, 2014.
- Robert K Katzschmann, Andrew D Marchese, and Daniela Rus. Autonomous object manipulation using a soft planar grasping manipulator. In *Under Review: Robotics and Automation (ICRA), 2015 IEEE International Conference on*. IEEE, 2015.
- Cecilia Laschi, Matteo Cianchetti, Barbara Mazzolai, Laura Margheri, Maurizio Follador, and Paolo Dario. Soft robot arm inspired by the octopus. *Advanced Robotics*, 26(7):709–727, 2012.
- Joel Lehman and Kenneth O Stanley. Evolving a diversity of virtual creatures through novelty search and local competition. In *Proceedings of the 13th annual conference on Genetic and evolutionary computation*, pages 211–218. ACM, 2011.
- Hod Lipson. Challenges and Opportunities for Design, Simulation, and Fabrication of Soft Robots. *Soft Robotics*, 1(P):21–27, 2013.
- Hod Lipson. Challenges and opportunities for design, simulation, and fabrication of soft robots. *Soft Robotics*, 1(1):21–27, 2014.
- Carmel Majidi. Soft robotics: A perspectivecurrent trends and prospects for the future. *Soft Robotics*, 1(1):5–11, 2014.
- Andrew D. Marchese. *Design, Fabrication and Control of Soft Robot using Fluidic Elastomer Actuators*. PhD thesis, MIT, 2014.
- Andrew D Marchese and Daniela Rus. Design, kinematics, and control of a soft spatial fluidic elastomer manipulator. In *Under Review: International Journal of Robotics Research*, 2015.
- Andrew D Marchese, Cagdas D Onal, and Daniela Rus. Soft robot actuators using energy-efficient valves controlled by electropermanent magnets. In *Intelligent Robots and Systems (IROS), 2011 IEEE/RSJ International Conference on*, pages 756–761. IEEE, 2011.
- Andrew D Marchese, Robert K Katzschmann, and Daniela Rus. Whole arm planning for a soft and highly compliant 2d robotic manipulator. In *Intelligent Robots and Systems*

- (*IROS*), 2011 IEEE/RSJ International Conference on. IEEE, 2014a.
- Andrew D Marchese, Konrad Komorowski, Cagdas D Onal, and Daniela Rus. Design and control of a soft and continuously deformable 2d robotic manipulation system. In *Proceedings of IEEE International Conference on Robotics and Automation*. IEEE, 2014b.
- Andrew D Marchese, Cagdas D Onal, and Daniela Rus. Autonomous soft robotic fish capable of escape maneuvers using fluidic elastomer actuators. *Soft Robotics*, 1(1):75–87, 2014c.
- Andrew D Marchese, Robert K Katzschmann, and Daniela Rus. Control and planning for soft planar fluidic elastomer manipulators. In *Under Review: International Journal of Robotics Research*, 2015a.
- Andrew D Marchese, Russ Tedrake, and Daniela Rus. Dynamics and trajectory optimization for a soft spatial fluidic elastomer manipulator. In *Under Review: Robotics and Automation (ICRA), 2015 IEEE International Conference on*. IEEE, 2015b.
- Ramses V Martinez, Jamie L Branch, Carina R Fish, Lihua Jin, Robert F Shepherd, Rui Nunes, Zhigang Suo, and George M Whitesides. Robotic tentacles with three-dimensional mobility based on flexible elastomers. *Advanced Materials*, 25(2):205–212, 2013.
- M. A. McEvoy and N. Correll. Shape change through programmable stiffness. In *International Symposium on Experimental Robotics (ISER)*, Marrakech, Morocco, 2014a. Springer Verlag.
- M Andy McEvoy and Nikolaus Correll. Thermoplastic variable stiffness composites with embedded, networked sensing, actuation, and control. *Journal of Composite Materials*, page 0021998314525982, 2014b.
- William McMahan, Bryan A Jones, and Ian D Walker. Design and implementation of a multi-section continuum robot: Air-octor. In *Intelligent Robots and Systems, 2005.(IROS 2005). 2005 IEEE/RSJ International Conference on*, pages 2578–2585. IEEE, 2005.
- William McMahan, V Chitrakaran, M Csencsits, D Dawson, Ian D Walker, Bryan A Jones, M Pritts, D Dienno, M Grissom, and Christopher D Rahn. Field trials and testing of the octarm continuum manipulator. In *Robotics and Automation, 2006. ICRA 2006. Proceedings 2006 IEEE International Conference on*, pages 2336–2341. IEEE, 2006.
- Stephen A Morin, Robert F Shepherd, Sen Wai Kwok, Adam A Stokes, Alex Nemirovski, and George M Whitesides. Camouflage and display for soft machines. *Science*, 337(6096):828–832, 2012.
- Bobak Mosadegh, Panagiotis Polygerinos, Christoph Keplinger, Sophia Wennstedt, Robert F Shepherd, Unmukt Gupta, Jongmin Shim, Katia Bertoldi, Conor J Walsh, and George M Whitesides. Pneumatic networks for soft robotics that actuate rapidly. *Advanced Functional Materials*, 24(15):2163–2170, 2014.
- Cagdas D Onal and Daniela Rus. A modular approach to soft robots. In *Biomedical Robotics and Biomechatronics (BioRob), 2012 4th IEEE RAS & EMBS International Conference on*, pages 1038–1045. IEEE, 2012.
- Cagdas D Onal and Daniela Rus. Autonomous undulatory serpentine locomotion utilizing body dynamics of a fluidic soft robot. *Bioinspiration & biomimetics*, 8(2):026003, 2013.
- Cagdas D Onal, Xin Chen, George M Whitesides, and Daniela Rus. Soft mobile robots with on-board chemical pressure generation. In *International Symposium on Robotics Research (ISRR)*, 2011.
- Yong-Lae Park, Bor-rong Chen, Néstor O Pérez-Arcibia, Diana Young, Leia Stirling, Robert J Wood, Eugene C Goldfield, and Radhika Nagpal. Design and control of a bio-inspired soft wearable robotic device for ankle–foot rehabilitation. *Bioinspiration & biomimetics*, 9(1):016007, 2014.
- Panagiotis Polygerinos, Stacey Lyne, Zheng Wang, Luis Fernando Nicolini, Bobak Mosadegh, George M Whitesides, and Conor J Walsh. Towards a soft pneumatic glove for hand rehabilitation. In *Intelligent Robots and Systems (IROS), 2013 IEEE/RSJ International Conference on*, pages 1512–1517. IEEE, 2013.
- Michael B Pritts and Christopher D Rahn. Design of an artificial muscle continuum robot. In *Robotics and Automation, 2004. Proceedings. ICRA'04. 2004 IEEE International Conference on*, volume 5, pages 4742–4746. IEEE, 2004.
- Daniela Rus and Michael T. Tolley. Soft: A New Paradigm in Robotics. *Under Review: Nature*, 2014.
- Sangok Seok, Cagdas Denizel Onal, Robert Wood, Daniela Rus, and Sangbae Kim. Peristaltic locomotion with antagonistic actuators in soft robotics. In *Robotics and Automation (ICRA), 2010 IEEE International Conference on*, pages 1228–1233. IEEE, 2010.
- Robert F Shepherd, Filip Ilievski, Wonjae Choi, Stephen A Morin, Adam A Stokes, Aaron D Mazzeo, Xin Chen, Michael Wang, and George M Whitesides. Multigait soft robot. *Proceedings of the National Academy of Sciences*, 108(51):20400–20403, 2011.
- Robert F Shepherd, Adam A Stokes, Jacob Freake, Jabulani Barber, Phillip W Snyder, Aaron D Mazzeo, Ludovico Cademartiri, Stephen A Morin, and George M Whitesides. Using explosions to power a soft robot. *Angewandte Chemie*, 125(10):2964–2968, 2013a.
- Robert F Shepherd, Adam A Stokes, Rui Nunes, and George M Whitesides. Soft machines that are resistant to puncture and that self seal. *Advanced Materials*, 25(46):6709–6713, 2013b.

- Adam A Stokes, Robert F Shepherd, Stephen A Morin, Filip Ilievski, and George M Whitesides. A hybrid combining hard and soft robots. *Soft Robotics*, 1(1):70–74, 2014.
- Koichi Suzumori, Shoichi Iikura, and Hiroshima Tanaka. Applying a flexible microactuator to robotic mechanisms. *Control Systems, IEEE*, 12(1):21–27, 1992.
- Koichi Suzumori, Satoshi Endo, Takefumi Kanda, Naomi Kato, and Hiroyoshi Suzuki. A bending pneumatic rubber actuator realizing soft-bodied manta swimming robot. In *Robotics and Automation, 2007 IEEE International Conference on*, pages 4975–4980. IEEE, 2007.
- Michael T Tolley, Robert F Shepherd, Michael Karpelson, Nicholas W Bartlett, Kevin C Galloway, Michael Wehner, Rui Nunes, George M Whitesides, and Robert J Wood. An untethered jumping soft robot. In *Intelligent Robots and Systems (IROS 2014), 2014 IEEE/RSJ International Conference on*, pages 561–566. IEEE, 2014a.
- Michael T Tolley, Robert F Shepherd, Bobak Mosadegh, Kevin C Galloway, Michael Wehner, Michael Karpelson, Robert J Wood, and George M Whitesides. A resilient, untethered soft robot. *Soft Robotics*, 2014b. ahead of print.
- Bertrand Tondu and Pierre Lopez. Modeling and control of mckibben artificial muscle robot actuators. *Control Systems, IEEE*, 20(2):15–38, 2000.
- Barry Trimmer. A journal of soft robotics: Why now? *Soft Robotics*, 1(1):1–4, 2014.
- Barry A Trimmer, Ann E Takesian, Brian M Sweet, Chris B Rogers, Daniel C Hake, and Daniel J Rogers. Caterpillar locomotion: a new model for soft-bodied climbing and burrowing robots. In *7th International Symposium on Technology and the Mine Problem*, volume 1, pages 1–10. Mine Warfare Association Monterey, CA, 2006.
- Deepak Trivedi, Christopher D Rahn, William M Kier, and Ian D Walker. Soft robotics: Biological inspiration, state of the art, and future research. *Applied Bionics and Biomechanics*, 5(3):99–117, 2008.
- T. Umedachi, V. Vikas, and B.A. Trimmer. Highly deformable 3-d printed soft robot generating inching and crawling locomotions with variable friction legs. In *Intelligent Robots and Systems (IROS), 2013 IEEE/RSJ International Conference on*, pages 4590–4595, Nov 2013. doi: 10.1109/IROS.2013.6697016.
- Pablo Valdivia y Alvarado and Kamal Youcef-Toumi. Design of machines with compliant bodies for biomimetic locomotion in liquid environments. *Journal of dynamic systems, measurement, and control*, 128:3, 2006.
- Hesheng Wang, Weidong Chen, Xiaojin Yu, Tao Deng, Xiaozhou Wang, and Rolf Pfeifer. Visual servo control of cable-driven soft robotic manipulator. In *Intelligent Robots and Systems (IROS), 2013 IEEE/RSJ International Conference on*, pages 57–62. IEEE, 2013.
- Michael Wehner, Michael T Tolley, Yiğit Mengüç, Yong-Lae Park, Annan Mozeika, Ye Ding, Cagdas Onal, Robert F Shepherd, George M Whitesides, and Robert J Wood. Pneumatic energy sources for autonomous and wearable soft robotics. *Soft Robotics*.
- Younan Xia and George M Whitesides. Soft lithography. *Annual review of materials science*, 28(1):153–184, 1998.